ASME GT2014-27094

INVESTIGATION OF UNSTEADY FLOW FIELD IN A LOW-SPEED ONE AND A HALF STAGE AXIAL COMPRESSOR, PART 2: EFFECTS OF TIP GAP SIZE ON THE TIP CLEARANCE FLOW STRUCTURE AT NEAR STALL OPERATION

Chunill Hah[1], Michael Hathaway[1], and Joseph Katz[2]
[1]NASA Glenn Research Center,
MS 5-10, Cleveland, Ohio
[2]Johns Hopkins University, Baltimore, Maryland

The primary focus of this paper is to investigate the effect of rotor tip gap size on how the rotor unsteady tip clearance flow structure changes in a low speed one and half stage axial compressor at near stall operation (for example, where maximum pressure rise is obtained). A Large Eddy Simulation (LES) is applied to calculate the unsteady flow field at this flow condition with both a small and a large tip gaps. The numerically obtained flow fields at the small clearance matches fairly well with the available initial measurements obtained at the Johns Hopkins University with 3-D unsteady PIV in an index-matched test facility which renders the compressor blades and casing optically transparent. With this setup, the unsteady velocity field in the entire flow domain, including the flow inside the tip gap, can be measured. The numerical results are also compared with previously published measurements in a low speed single stage compressor (Maerz et al. [2002]). The current study shows that, with the smaller rotor tip gap, the tip clearance vortex moves to the leading edge plane at near stall operating condition, creating a nearly circumferentially aligned vortex that persists around the entire rotor. On the other hand, with a large tip gap, the clearance vortex stays inside the blade passage at near stall operation.

With the large tip gap, flow instability and related large pressure fluctuation at the leading edge are observed in this one and a half stage compressor. Detailed examination of the unsteady flow structure in this compressor stage reveals that the flow instability is due to shed vortices near the leading edge, and not due to a three-dimensional separation vortex originating from the suction side of the blade, which is commonly referred to during a spike-type stall inception. The entire tip clearance flow is highly unsteady. Many vortex structures in the tip clearance flow, including the sheet vortex system near the casing, interact with each other. The core tip clearance vortex, which is formed with the rotor tip gap flows near the leading edge, is also highly unsteady or intermittent due to pressure oscillations near the leading edge and varies from passage to passage. For the current compressor stage, the evidence does not seem to support that a classical vortex breakup occurs in any organized way, even with the large tip gap. Although wakes from the IGV influence the tip clearance flow in the rotor, the major characteristics of rotor tip clearance flows in isolated or single stage rotors are observed in this one and a half stage axial compressor.

INTRODUCTION

It is well known that tip clearance flow plays an important role in the operation of axial compressors. When the tip clearance becomes large during the service life of an engine, both the efficiency at the design condition and the stall margin deteriorate. Many experimental and analytical studies to understand tip clearance flows have been reported (for example, Hah [1987], Hoeing et al. [1993], Vo et al. [1998], Inoue et al. [2004], Chen et al. [2008], Weichert and Day [2012], Yamada et al. [2013], etc.). However the tip clearance flow at near stall operation, especially unsteady characteristics in a multi-stage environment, is not fully understood.

Tip clearance flow arises due to the pressure difference between the pressure and suction sides of the blade in the tip gap area. Flow through the tip gap interacts with the incoming passage flow near the suction side of the blade as it leaves the blade tip section, forming the tip clearance vortex. The vortex core is formed by fluid originating from near the leading edge of the blade. Fluid flowing over the remainder of the blade rolls around this core vortex and adds swirl intensity. Some tip clearance flow originating near the casing travels over to the tip gap of the adjacent blade, resulting in so-called double leakage flow (Smith [1993]). Tip clearance flow has been handled as a steady flow phenomenon for many applications. However, tip clearance flow in a compressor is not steady even at design operation due to vortex shedding at the trailing edge and oscillation of the tip leakage vortex, as well as flow field interactions from adjacent blade rows. Bergner et al. [2006] measured the instantaneous pressure difference between the blade suction side and pressure side near the leading edge at near stall operation. They reported that the pressure difference changes constantly and the pressure difference occasionally becomes

even negative during near stall operation, which indicates that the formation of the tip clearance flow is also transient and the tip leakage vortex itself is formed intermittently.

The effect of the rotor tip gap size on the compressor flow field has been widely investigated. Several previous studies (Mailach et al. [2000], Maertz et al. [2002], Kiel et al. [2003], Inoue et al. [2004], etc.) reported that rotating instability occurs when the tip gap is increased in axial compressors. As the resulting non-synchronous blade vibration affects engine safety, many studies have been reported. Maertz et al. [2002] reported movement of the instability vortex along the leading edge plane is the main cause of the instability during the compressor operation near stall. Inoue et al. [2004] and Yamada et al. [2013] reported formation of a tornado-type vortex near the suction surface and subsequent vortex breakup as the main mechanism of the flow at near stall operation with a large tip gap.

Although lately significant progress has been made in the experimental investigation of tip gap flow, direct measurement of the unsteady flow field inside the rotor tip gap has not been possible. A new program to investigate the unsteady tip clearance flow in a low speed one and a half stage axial compressor was initiated under the auspices of the NASA Fixed Wing Project to understand and mitigate losses associated with large rotor tip gaps of N+3 relevant small, high overall pressure ratio compressor aft stages. Detailed measurements of the unsteady tip clearance flows at two tip clearances (0.5 mm and 1.95 mm, 0.49% and 1.9% rotor tip chord) will be acquired with three-dimensional PIV in an index-matched test facility at the Johns Hopkins University. Details of the PIV procedure are given by Wu et al. [2011]. The primary focus of the program is to study the detailed unsteady flow structures in the tip gap at the design and near stall operation. The measured data will be used to study loss generation mechanisms with different clearance levels and to validate unsteady CFD. The compressor geometry and all related data will be available to the research technical community.

The present paper reports numerical investigation of the rotor tip clearance flows for this one and a half stage axial compressor. The primary focus of the current study is to investigate detailed tip clearance flow mechanisms in the one and a half stage axial compressor at two tip gaps. The LES numerical results are used as a reference for the PIV experimental campaign, which will be used to aid further analysis of the LES results.

ONE AND A HALF STAGE LOW SPEED AXIAL COMPRESSOR FOR TIP GAP FLOW RESEARCH

The design intent for the John's Hopkins University (JHU) compressor, which is focused on investigating the flow physics of the rotor tip clearance flow field, was for it to be an aerodynamically scaled derivative of the first 1 and 1/2 stages (i.e., inlet guide vane, rotor, and stator) of the NASA Glenn Research Center's Low-Speed Axial Compressor (LSAC), which comprises an IGV followed by four geometrically identical stages designed for accurate low-speed simulation of a high-speed multistage core compressor (Wasserbauer, 1995). In addition, commensurate with the NASA LSAC compressor, the JHU compressor should have a long entrance length to develop thick endwall boundary layers typical of an embedded stage. The NASA LSAC blades themselves were aerodynamically scaled and modeled after General Electric's Energy Efficient Engine blading (Wisler, 1977), with modifications to the original GE blade geometry to account for differences in the hub-to-tip ratios of the two compressors (Wellborn, 1996). The JHU, LSAC, and GE compressor design heritage therefore provides potential for continuity of physics insight obtained from these related, but different compressors. The JHU compressor was sized to a 9" (22.86 cm) casing flow path radius to be compatible with the JHU compressor facility hardware, and was initially mechanically scaled from the NASA LSAC 24" (60.96 cm) casing radius. However, a direct mechanical scale yields a rotor blade tip thickness that was too thin to withstand the stresses associated with operation in the much higher density NaI-H2O mixture of the working fluid at the desired 480 rpm design speed set by the facility power limitations. It was therefore necesary to increase the rotor blade tip thickness to 0.169" (4.3 mm) to withstand the higher stress at the rotor blade tip. Then, to maintain the LSAC rotor blade profile shape, and thus aerodynamic similarity with the LSAC, the JHU rotor was fixed to have the same rotor blade tip thickness to chord ratio as the NASA LSAC, and the rotor tip chord increased to achieve a 0.169" (4.3 mm) rotor blade tip thickness. The resultant rotor chord scaling was then used for the IGV, rotor, and stator, which yielded a longer axial chord, relative to a direct mechanical scale, and thus a much lower aspect ratio. Next, to maintain rotor tip solidity (recall focus of JHL rig is the rotor tip clearance flow physics) the number of IGV, rotor, and stator blades were decreased, and then fixing the rotor count the IGV and Stator counts were slightly adjusted to achieve a 20 IGV, 15 rotor, and 20 stator blade count, which with a 3/4 ratio of rotor to IGV/Stator blade passages facilitates unsteady simulations. The target Reynolds number is 4.0×10^5 based on tip speed and the rotor chord length at tip. Details of the design parameters are given by Tan et al. [2014].

Figure 1 shows the cross section of the test compressor. A view of the compressor test section is given in Figure 2. Two rotor blade tip gaps of 0.5 mm (0.49 % of tip chord) and 1.95 mm (1.9 % of tip chord) were selected for the study. The compressor static pressure rise characteristic curve for the 0.5 mm tip gap is given in Figure 3. LES simulations were performed at near stall operation with two tip gaps and the calculated static pressure rises are marked in Figure 3.

NUMERICAL PROCEDURE

A Large Eddy Simulation (LES) was applied in the present study to calculate the unsteady flow and various vortex structures in the rotor tip gap. With spatially-filtered Navier-Stokes equations, the subgrid-scale stress tensor term must be modeled properly for closure of the governing

equations. A Smagorinsky-type eddy-viscosity model was used for the subgrid stress tensor, and the standard dynamic model by Germano et al. [1991] was applied.

In the current study, the governing equations are solved with a pressure-based implicit method using a fully conservative control volume approach. A third-order accurate interpolation scheme is used for the discretization of convection terms and central differencing is used for the diffusion terms. The method is of second-order accuracy with smoothly varying grids. For the time-dependent terms, an implicit second-order scheme is used and a number of sub-iterations are performed at each time step. About 6000 time steps are used for one rotor revolution.

Standard boundary conditions for the multi-blade rows were applied at the boundaries of the computational domain (Hah and Shin [2010]). The inflow boundary of the computational domain was located 20 average blade heights upstream of the rotor leading edge in order to damp out any possible reflections. Likewise, the outflow boundary was located 20 blade heights downstream from the trailing edge. Circumferentially averaged static pressure at the exit boundary casing was specified to control the mass flow rate. Non-reflecting boundary conditions were applied at the inlet and the exit boundaries.

The computational grid consists of 194 nodes in the blade-to-blade direction, 128 nodes in the spanwise direction, and 280 nodes in the streamwise direction for each blade passage. The rotor tip clearance geometry is represented by 28 nodes in the blade-to-blade direction, 16 nodes in the spanwise direction, and 180 nodes in the streamwise direction in an attempt to accurately resolve the tip clearance flow field. I-grid topology is used to reduce grid skewness and a single-block grid is used. For the current study of the flow field at near stall operation, all the flow passages were solved although the number of blades could be reduced from 20-15-20 to 4-3-4 if periodicity condition is applied. The grid size for the entire one and half stage with all the blade passages is about 380 million nodes. The wall resolution is within the range $Dx^+ < 40$, $Dy^+ < 1.2$, and $Dz^+ < 2.0$ in streamwise, pitchwise, and spanwise directions. The applied grid is not fine enough to resolve small length scales in the wall boundary layer. However, the current study is aimed to investigate tip clearance flow which is formed away from the wall. Figure 4 shows the computational grid near the compressor stage.

All the computations were performed with NASA's Columbia supercomputer system, which allows parallel computation with up to 512 processors.

TIP CLERANCE FLOW WITH A SMALL TIP GAP AT NEAR STALL OPERATION

Figure 5 shows the predicted distribution of instantaneous pressure at the rotor tip section with the small tip gap at near stall operation. The instantaneous pressure distribution in Figure 5 shows minor variation of flow structures among the blade passages. At this flow condition, there is no sign of any stall inception and no indication of flow separation near the suction side of the blade. Detailed instantaneous pressure distribution in one of the rotor passages is shown in Figure 6(a). Many vortex structures are observed in Figure 6(a) in addition to the tip clearance vortex. Tip clearance vortex ropes are clearly shown in Figure 6(a). Instantaneous velocity vectors along with instantaneous pressure contours are given in Figure 6(b).

Corresponding flow visualization of the tip clearance flow obtained from the JHU tests as indicated with small cavitation bubbles is given in Figure 7. As the cavitation inception occurs due to low pressure, the cavitation in Figure 7 shows low pressure distribution. The rotor tip clearance core vortex and many vortex structures due the interaction between tip gap flow and main flow near the suction side downstream of the leading edge are clearly depicted in Figure 7. The low pressure area near the suction surface toward the casing is also shown in Figure 7. However, no flow separation near the suction surface is observed.

The predicted tip vortex structures from the LES simulations shown in Figure 6 agree well with the flow visualization results from the JHU tests shown in Figure 7. Both the flow visualization and the LES clearly show the tip clearance vortex rope. The LES predicted time-averaged pressure and velocity fields at the rotor tip section are given in Figures 8 and 9. With the small tip gap, the tip clearance vortex is moved up to the blade leading edge plane. Figure 10 shows the standard deviation of static pressure at the rotor tip section and instantaneous axial velocity contours. Large fluctuations near the blade leading edge in Figure 10 are due to the interaction with the incoming IGV wakes as shown in the axial velocity contours.

TIP CLEARANCE FLOW AT NEAR STALL OPERATION WITH A LARGE TIP GAP

The predicted instantaneous pressure field at the rotor tip section with the large tip gap at near stall operation is given in Figure 11. The pressure field in Figure 11 reveals a complex flow structure. The Instantaneous pressure field varies substantially among the different blade passages. The location and strength of the tip clearance vortex also vary significantly from one blade passage to another. Vortex structures with low pressure cores along the leading edge plane are located at several blade passages. Blade passages with typical tip clearance vortex structure are followed with blade passages with no clear tip vortex structure.

Time-lapse photos of the casing wall in a single stage axial compressor (Maerz et al. [2006]) at near stall operation with four different tip gaps (from 0.7 % to 5.6%) at maximum pressure rise are shown in Figure 12 for comparison purpose. The Maerz case of 2.8 % tip gap represents a similar flow field structure to the current tip gap from the LES simulations of the present study. Although there should be some effects of IGV wakes on the rotor tip flow in the current one and half stage compressor, the instantaneous pressure field from a single stage compressor shown in Figure 12 supports the numerical results shown in Figure 11.

Time-averaged pressure and velocity fields predicted from the LES simulations are shown in Figures 13 and 14. The time-averaged flow field shows a classical tip gap flow structure at near stall operation. The time-averaged pressure field shows more diffused tip clearance core vortex than that from a steady isolated rotor simulation. This is due to the oscillation of the tip clearance vortex and actual measurement of ensemble averaged wall pressures shows the same feature. The time averaged velocity field does not show either leading edge flow spillage or flow reversal at the trailing edge. As the compressor operates in stable mode without stall inception, the present flow validates the stall inception criteria of Vo et al. [2008].

The standard deviation of the predicted static pressure at the rotor tip section is given in Figure 15. An area of high fluctuation of the static pressure is shown along the leading edge plane. The magnitude of pressure fluctuation at the leading edge plane with the large tip gap in Figure 15 is quite different from that with the small tip gap shown in Figure 10. With the large tip gap, large pressure fluctuations are observed along the leading edge plane away from the blade surface. Figure 16 shows ensemble-averaged pressure and standard deviation of the static pressure from a low speed single stage compressor (Martz et al. [2002]). With the 0.7 % tip gap, which is similar tip gap with the current small tip gap, there is no pressure deviation near the leading edge plane as there is no IGV wake interaction. Again, very similar flow phenomena at the leading edge plane are observed with the large tip gap between the current one and a half stage compressor and the single stage compressor of Marz. Although wakes from the IGV influence the rotor tip flow, flow instability in the current one and a half stage compressor is very similar to that in the single stage compressor (Matz et al. [2002]).

The origin and detailed behavior of the flow instability with the large tip gap in the current compressor stage are examined in detail in the next section.

WHY ROTATING INSTABILITY ONLY WITH THE LARGE TIP GAP?

The time history of the predicted static pressure differences between the suction and the pressure side of the blade at 5% chord downstream from the leading edge are compared in Figure 17 for two tip gaps at near stall operation. The changes in pressure are about 10 times higher with the large tip gap than those with the small tip gap. The tip clearance flow is the direct result of pressure difference across the rotor blade tip section and the magnitude and the direction of the tip clearance flow depend on the pressure difference across the blade section.

As the pressure difference varies in time as shown in Figure 17, the tip clearance flow and the formation of the tip clearance vortex become transient. Changes in flow structure during the flow instability are shown in Figure 18. The vortex with the low pressure core originates near the blade suction side and moves to the pressure side. Changes of instantaneous pressure distribution in Figure 18 indicate that this instability vortex is the result of flow interaction with the main incoming flow, tip leakage flow, and reversed flow near the casing.

Instantaneous velocity vectors near the instability vortex are given in Figure 19. With the periodically changing pressure difference across the rotor blade section, the strength of the tip gap flow also changes and the instability vortex is created intermittently. Instantaneous pressure distributions at the rotor tip and at 75 % span in a rotor passage are compared in Figure 20. The pressure distribution at the 75% span in Figure 20 does not show any flow separation near the leading edge at this span.

The results in Figures 18, 19 and 20 indicate that the instability vortex does not originate from the leading edge flow separation and is not the same radial vortex observed during the spike-type stall inception (Pullan et al. [2012], Yamada et al. [2013]). As the compressor operates further into stall inception, a radial vortex system due to flow separation near the leading edge could develop. However, the instability vortices in the current study seem to be from the vortex shedding near the leading edge like previous studies (Matz et al. [2002] and Kielb et al. [2003]). The creation and movement of the instability vortex are rather random as shown in figure 18. The movement of this instability vortex is the main cause of the high pressure fluctuation along the leading edge plane shown in Figure 17. Tip clearance vortex structures shown in Figure 18 do not indicate any traditional vortex breakup. The formation and the transport of the tip clearance vortex are highly transient or intermittent due to the large pressure fluctuation at near stall operation. The tip clearance vortex does not seem to gain enough swirl intensity to have a traditional vortex breakup.

The power spectrum of the pressure near the leading edge is given in Figure 21. A large hump is observed at around 60 % of the blade passing frequency. This characteristic hump represents rotating flow instability with non-synchronous rotor vibration (Maerz et al. [2002]).

Although the flow instability and the resulting non-synchronous vibration have been reported in many compressors, no physical explanation has been provided as to why flow instability occurs with only larger tip gaps. Time averaged axial velocity distributions near the casing are compared between the two tip gaps in Figure 22. As shown in Figure 22, the casing boundary layer is separated over most of the blade passage for the large tip gap and reversed flow near the pressure side of the leading edge, which interact with the incoming flow to form the instability vortex. Larger variation of pressure difference near the leading edge (Fig.17) and more extensive reversed casing flow (Fig. 22) seem to be the main reason of the flow instability with the larger tip gap.

CONCLUDING REMARKS

The unsteady tip clearance flows in a low speed one and a half stage axial compressor with two tip gaps are investigated with a Large Eddy Simulation. The current

investigation is a part of a NASA research project supported by the Fixed Wing Project to study the effects of various tip gap sizes on the efficiency and stall margin in axial compressor. At the near stall operation, the rotor tip clearance flow becomes transient due to self-induced oscillation of the tip vortex in addition to blade row interactions. The pressure difference across the rotor blade section near the leading edge, which drives the tip clearance flow, also fluctuates significantly. Consequently, formation of the tip leakage core vortex becomes intermittent. With the large tip gap, this fluctuation of pressure difference near the rotor leading edge becomes much larger than that with the small tip gap and an instability vortex is formed near the leading edge. This instability vortex moves from the suction side of the blade to the pressure side of the blade, which results in large pressure fluctuations on the blade surface and the non-synchronous blade vibration phenomena. The instability vortex is the shed vortex from the suction side of the leading edge at the rotor tip. The instability vortex observed in the current study is not a tornado-type separation vortex, which is commonly referred to during the spike-type stall inception.

ACKNOWLEDGMENTS

The author gratefully acknowledge the support of this work by the NASA Fundamental Aeronautics program, Fixed Wing project.

REFERENCES

Bergner, J., Matthias, K, Schiffer, H.P., and Hah, C., 2006, “Short Length-Scale Rotating Stall Inception in a Transonic Axial Compressor – Experimental Investigation,” ASME Paper GT2006-90209.

Chen, J.P., Hathaway, M.D., and Herrick, G.P., 2008, “Prestall Behavior of a Transonic Axial Compressor Stage via Time-Accurate Numerical Simulation,” ASME Journal of Turbomachinery, Vol. 30,October 2008.

Germano, M., Piomelli, U., Moin, P., and Cabot, W. H., 1991, “A Dynamic Subgrid-Scale Eddy-Viscosity Model,” Journal of Fluid Mechanics, Vol. A3, pp. 170-176.

Hah, C., 1986, "A Numerical Modeling of Endwall and Tip-Clearance- Flow of an Isolated Compressor ," ASME Journal of Engineering for Gas Turbines and Power Vol. 108, No. 1, pp. 15-21.

Hah, C. and Shin, H., 2012, “Study of Near –Stall Flow Behavior in a Modern Transonic Fan with Compound Sweep,” ASME Journal of Fluids Engineering,Vol.134, pp.071101-071107.

Hoying,D.A., Tan, C.S., Vo, H.D., and Greitzer, E.M., 1999, “Role of blade passage flow structure in axial compressor rotating flow inception,” ASME J. of Turbomachinery, 121,pp.735-742.

Inoue, M., Kuromaru, M, Yoshida, S., Minami, T., Yamada, K., and Furukawa, M., 2004, “Effects of Tip Clearance on Stall Evolution Process in a Low-Speed Axial Compressor Stage,” ASME Paper GT2004-5335.

Kielb, R. E., Barter, J. W., Thomas, J., and Hall, K. C., 2003, “Blade Excitation by Aerodynamic Instabilities–A Compressor Blade Study,” ASME Paper GT2003-38634.

Maerz, J., Hah, C., and Neise, W, 2002, “An Experimental and Numerical Investigation into the Mechanism of Rotating Instability,” ASME Journal of Turbomachinery, Vol. 124, pp. 367-375.

Mailach, R., Lehmann, I., and Vogeler, K., 2000, "Rotating Instabilities in an Axial Compressor Originating from the Fluctuating Blade Tip Vortex," ASME Paper 2000-GT.

Pullan, G., Young, A.M., Day, I.J., Greitzer, E.M., Spakovszky, Z.S., 2013, “Origins and Structure of Spike-Type Rotating Stall,” ASME paper 2012-68707.

Smith L. H. Jr., 1993, Private communication.

Vo, H. D., Tan, C. S., and Greitzer, E. M., 2005, “Criteria for Spike Initiated Rotating Stall,” ASME Paper GT2005-68374.

Tan, D., Yuanchao, L., Wilkes, I., Miorini, R.L., and Katz, J., 2014, “Visualization and Time Resolved PIV Measurements of the Flow in the Tip region of a Subsonic Compressor Rotor,” ASME Paper GT2014-27195.

Yamada, K, Kikuda, H.,Furukawa, Kunjishima, S., and Hara, Y., 2013, “Effects of Tip Clearance on the Stall Inception Process in an Axial Compressor Rotor,” ASME Paper GT-2013-95479.

Wasserbauer, C. A., Weaver, H. F., and Senyitko, R. G., “NASA Low-Speed Axial Compressor for Fundamental Research, “ NASA TM 4635, Feb. 1995.

Weichert, S. and Day, I, 2013, “Detailed Measurements of Spike Formation in an Axial Compressor,” ASME paper GT2013.

Wellborn, S. R., Okiishi, T. H., “Effects of Shrouded Stator Cavity Flows on Multistage Axial Compressor Aerodynamic Performance, “ NASA Contractor Report 198536, October 1996.

Wisler, D. C., “Core Compressor Exit Stage Study: Volume 1- Blade Design,” NASA CR

Wu, H., Tan, D., Miorini, R.L., and Katz, J., 2011, “Three-Dimensional Flow Structures and Associated Turbulence in the Tip Region of a Water Jet Pump Rotor,”Exp. Fluids, 51(6), pp. 1721-1737.

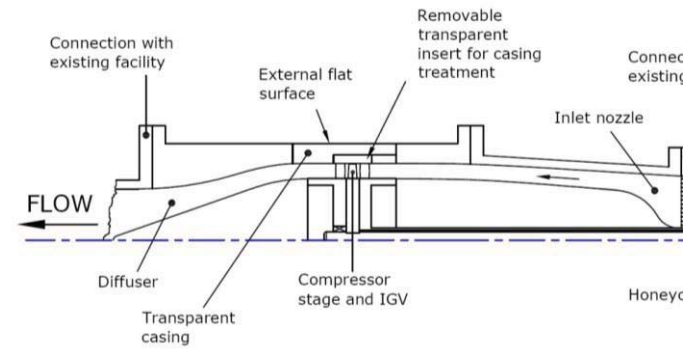

Figure 1: Cross section of the test compressor facility.

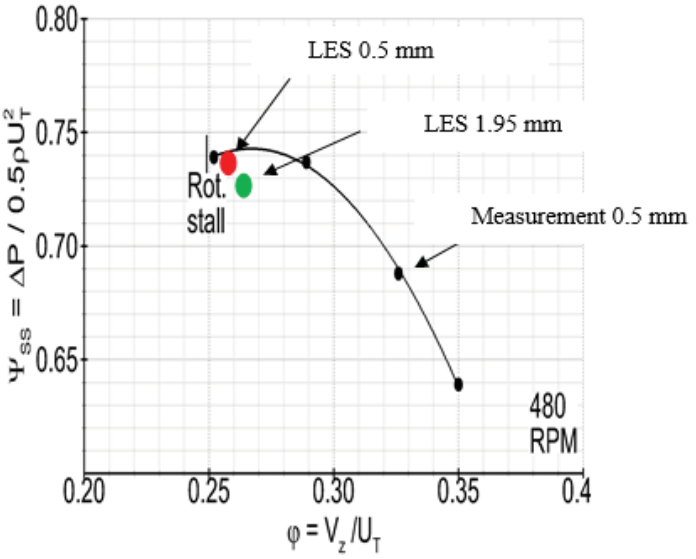

Figure 3: Pressure rise characteristics.

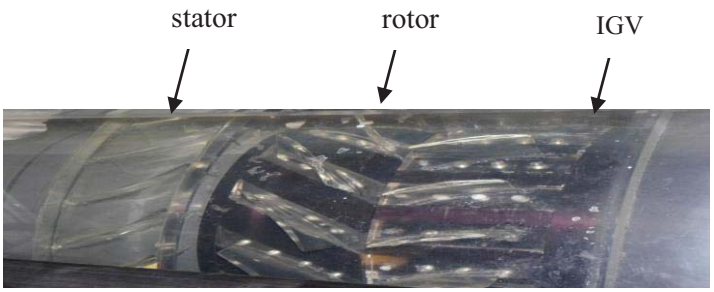

Figure 2: View of index-matched transparent compressor stage.

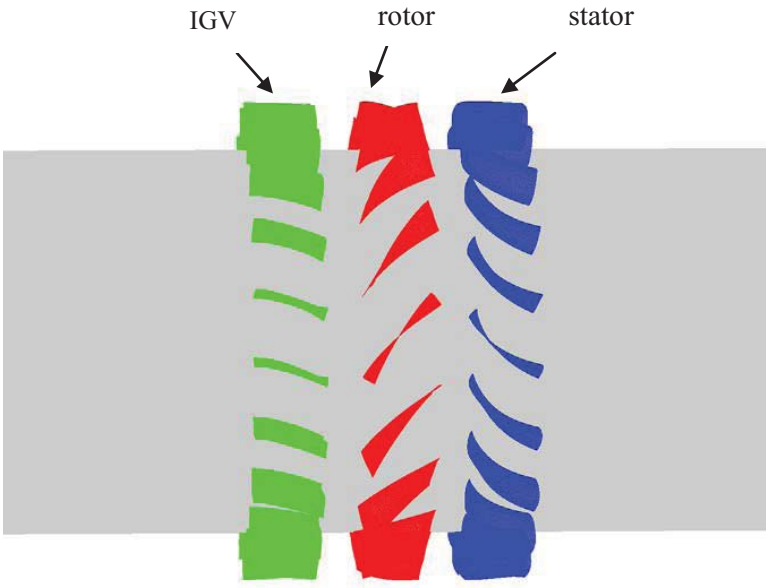

Figure 4: Computational grid near the blades.

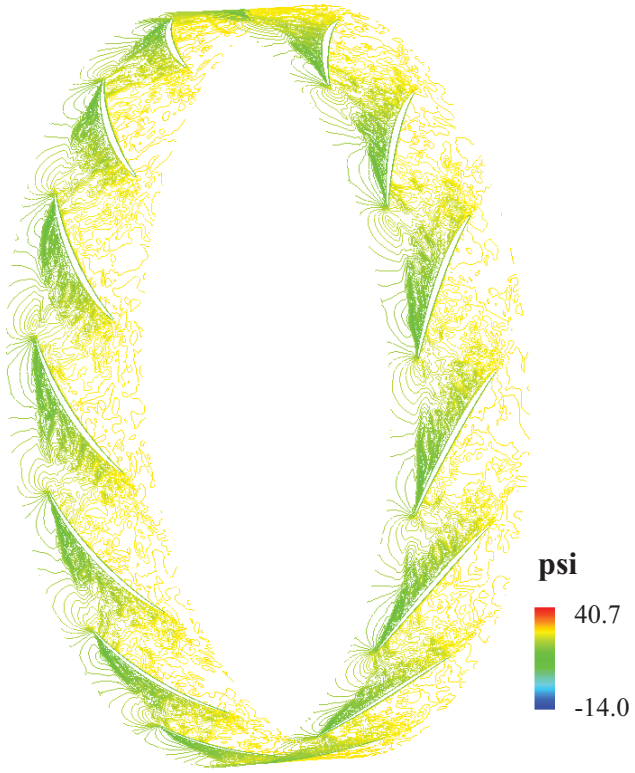

Figure 5: Instantaneous pressure distribution at rotor tip, near stall, 0.5 mm tip gap.

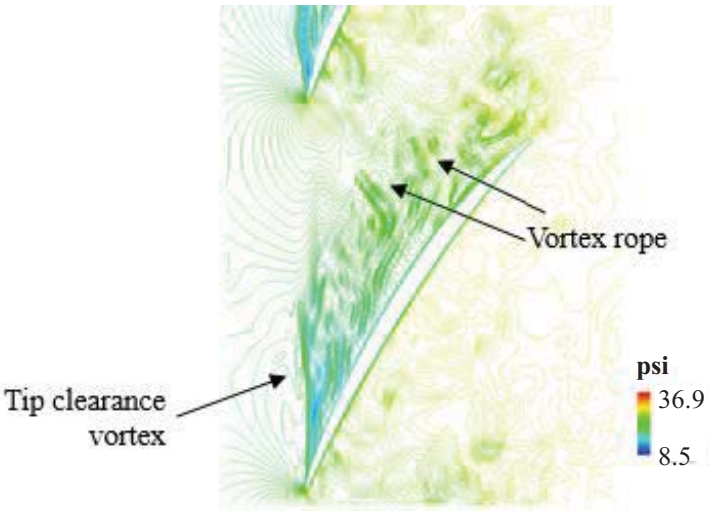

Figure 6(a): Detailed instantaneous pressure distribution, rotor tip, near stall, 0.5mm tip gap.

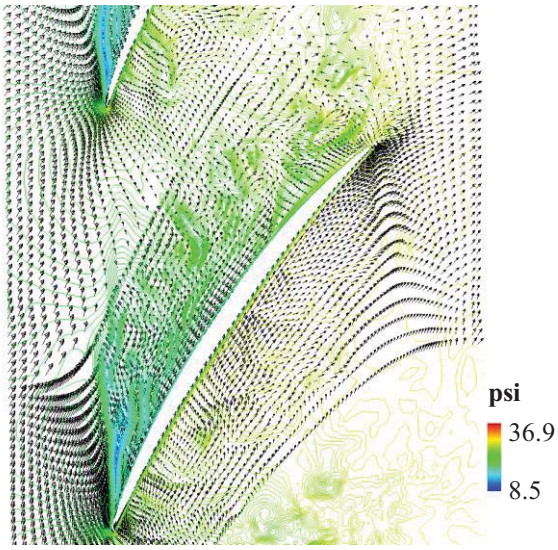

Figure 6(b): Detailed instantaneous velocity distribution, rotor tip, near stall, 0.5 mm tip gap

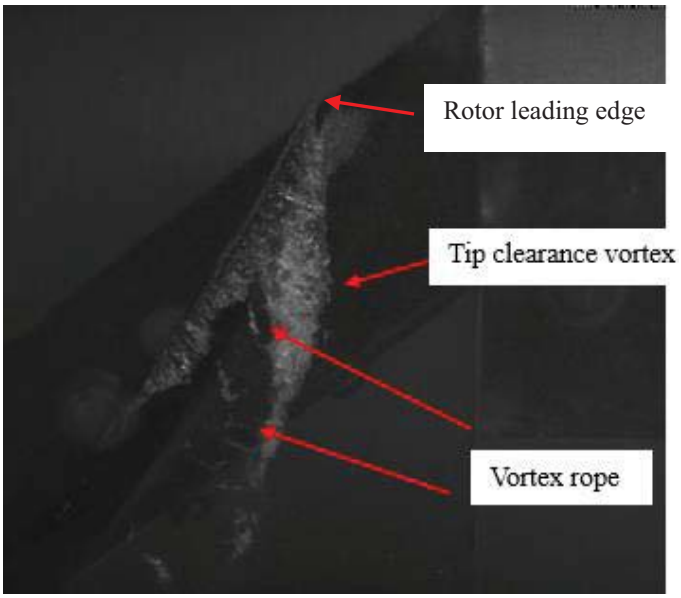

Figure 7: Flow visualization of instantaneous pressure field via cavitation measurement with a high speed camera.

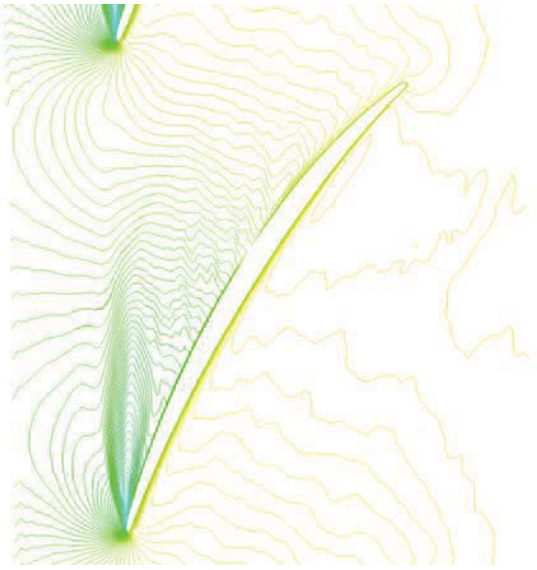

Figure 8: Time-averaged pressure field, rotor tip, near stall, 0.5 mm tip gap.

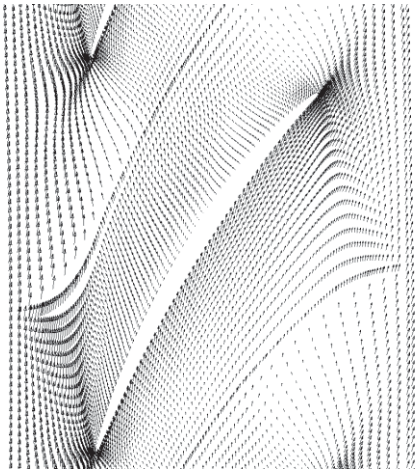

Figure 9: Time-averaged velocity field, rotor tip, near stall, 0.5 mm tip gap.

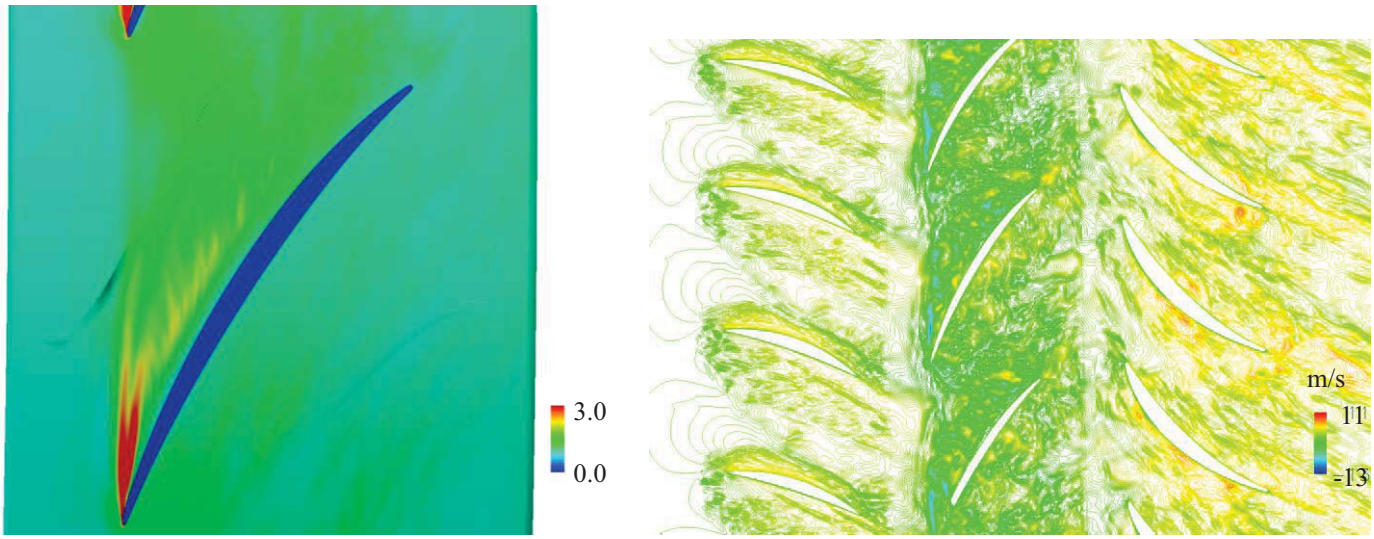

Standard deviation

Instantaneous axial velocity contours

Figure 10: Standard deviation of static pressure and instantaneous axial velocity contours at rotor tip, near stall, 0.5 mm tip gap.

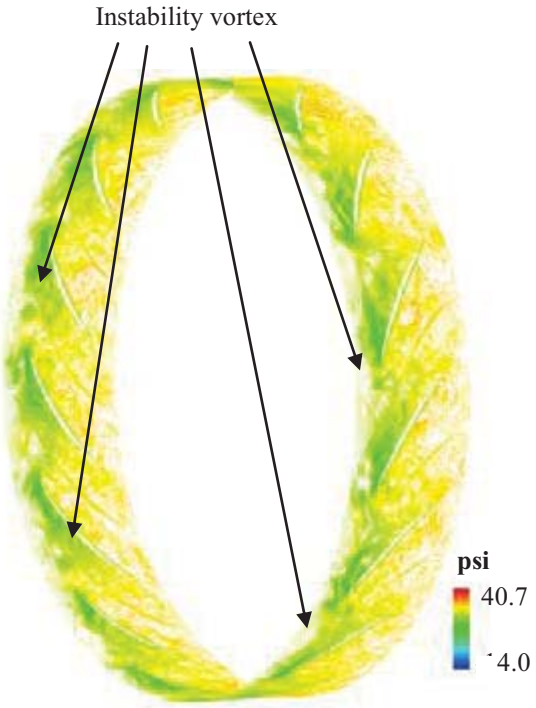

Figure 11: Instantaneous pressure distribution at rotor tip, near stall, 1.95 mm tip gap.

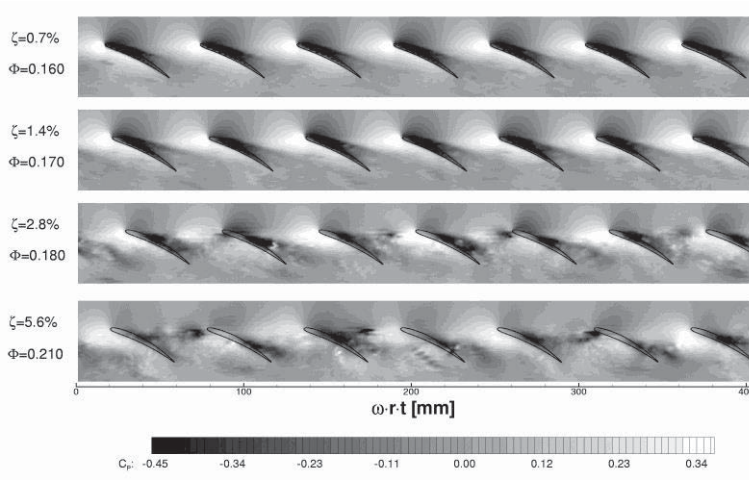

Figure 12: Time-lapsed plots of casing wall pressure at near stall with different tip clearances from a single stage compressor (Marz et al. [2002]).

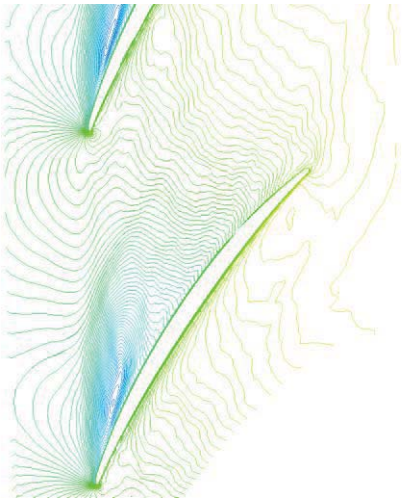

Figure 13: time-averaged pressure distribution at rotor tip, near stall, 1.95 mm tip gap.

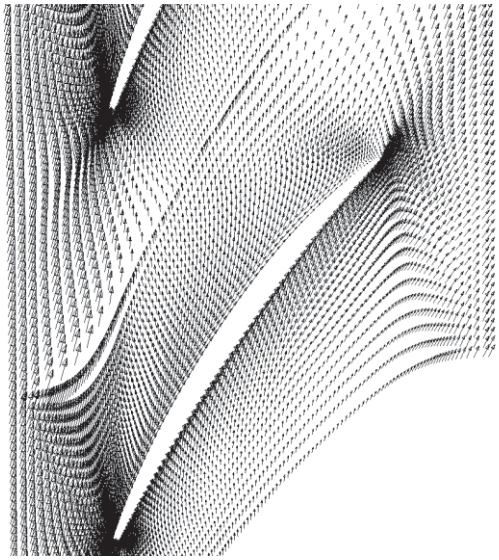

Figure 14: Time-averaged velocity field at rotor tip, near stall, 1.95 mm tip gap.

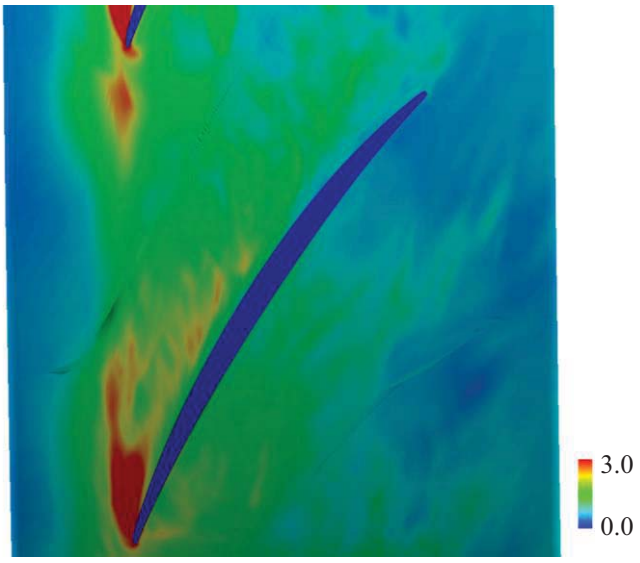

Figure 15: Standard deviation of static pressure at rotor tip, near stall, 1.95 mm tip gap.

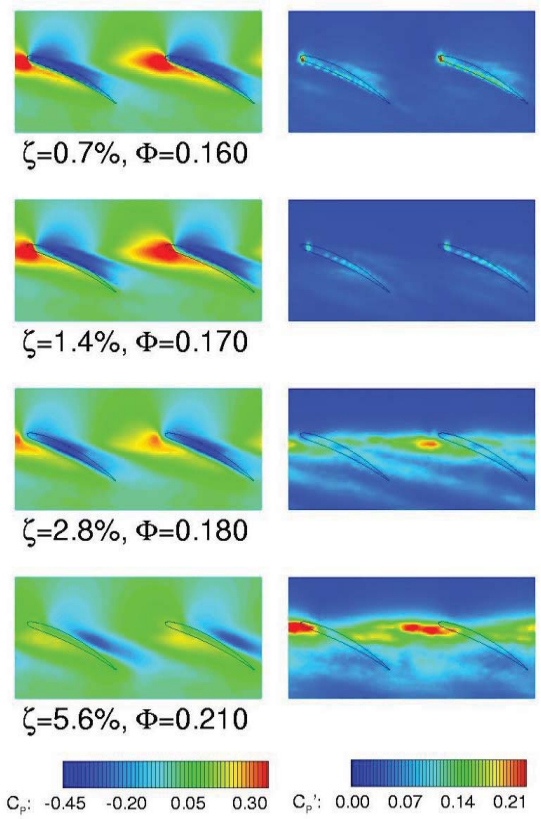

Figure 16: Ensemble averages and standard deviation of static pressure at rotor tip, near stall with different clearances from a single stage compressor (Marz et al. [2002])

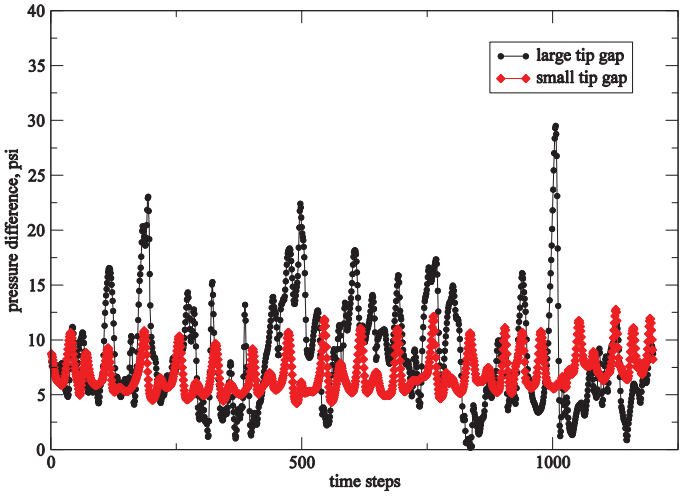

Figure 17: Changes of the pressure difference across blade near leading edge, rotor tip with two rotor tip gap

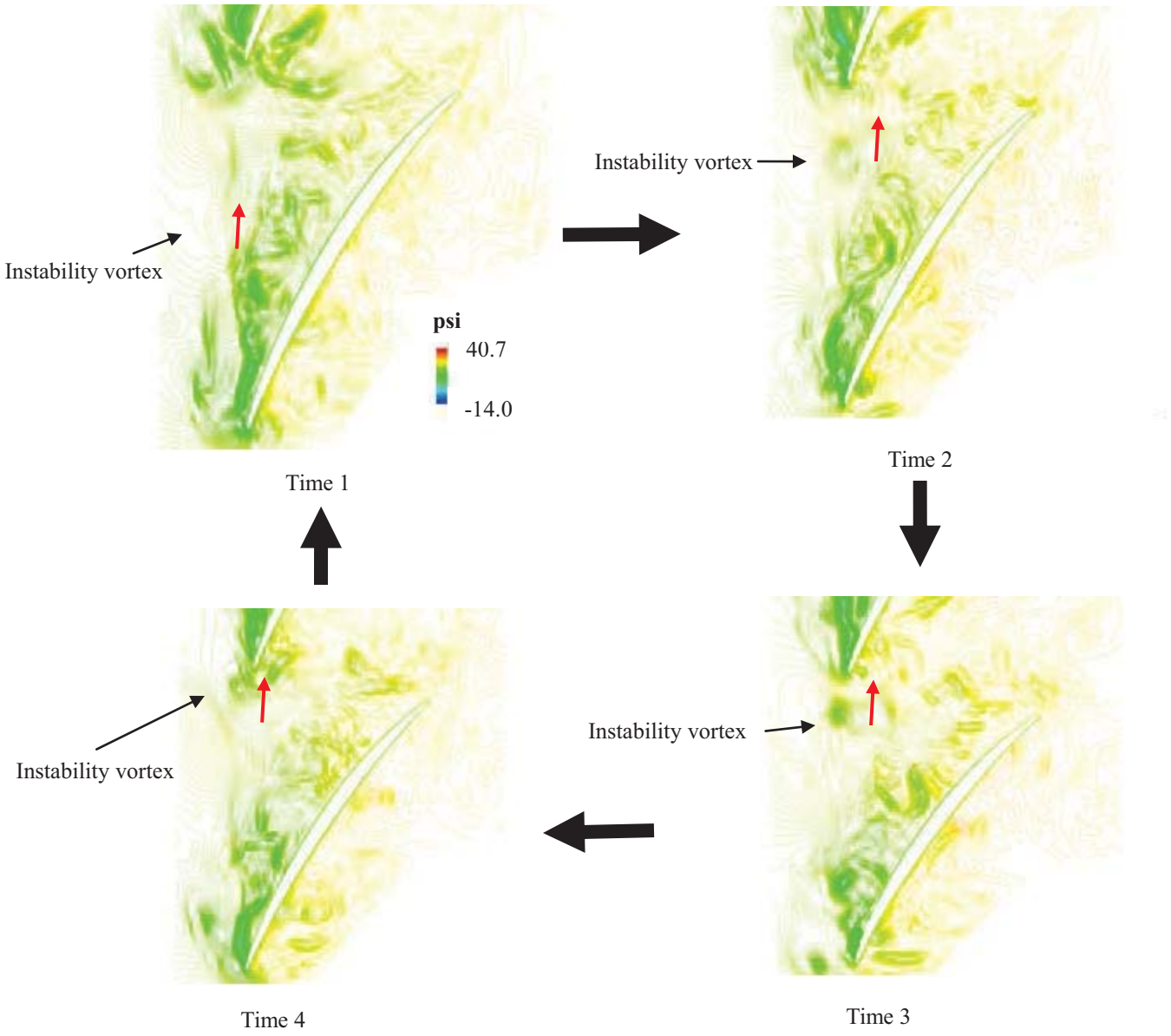

Figure 18: Development of instability vortex (changes in pressure field, rotor tip, near stall, 1.95 mm tip gap).

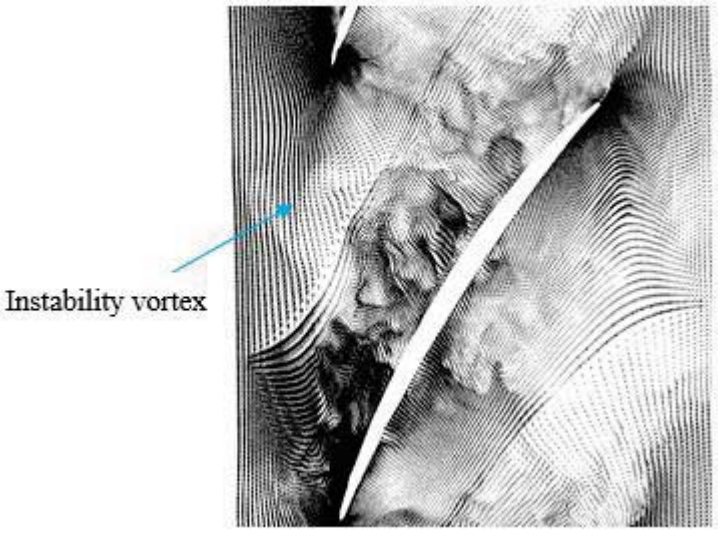

Figure 19: Instantaneous velocity vectors near the instability vortex.

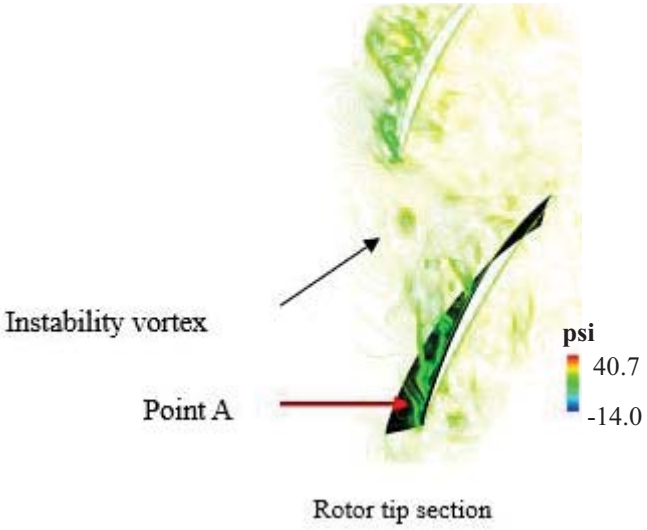

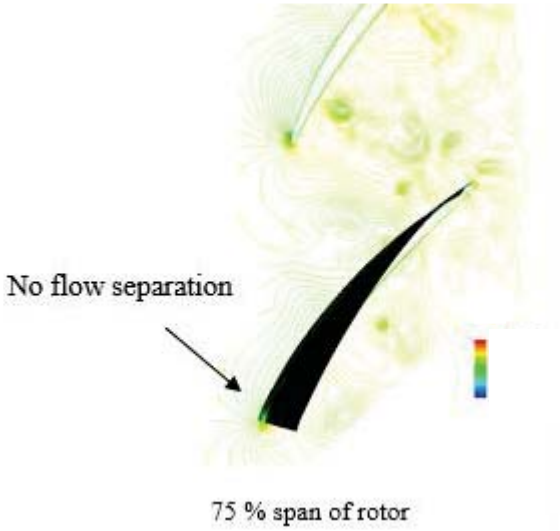

Figure 20: Comparison of instantaneous pressure distribution between rotor tip section and 75 % span, near stall, 1.95 mm tip gap.

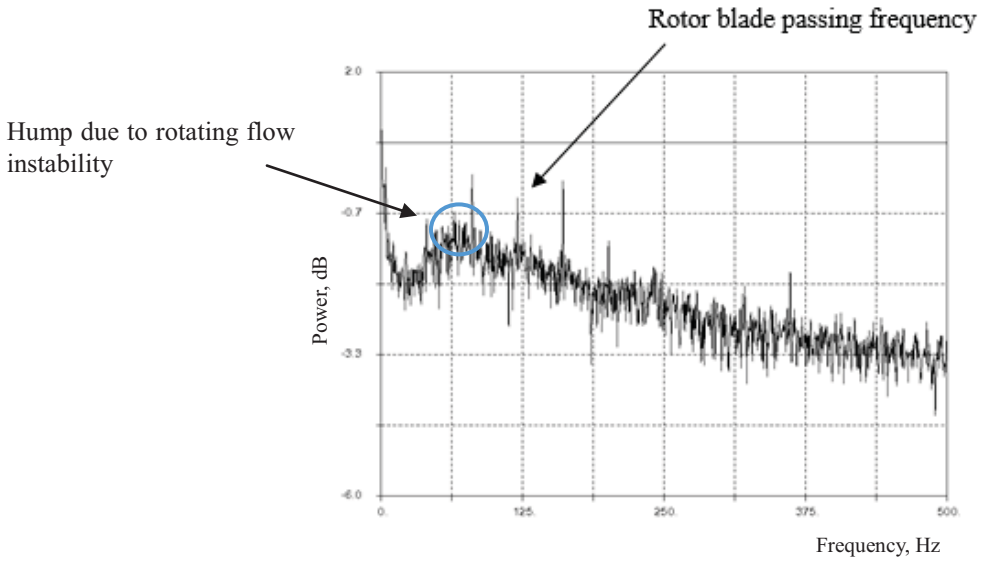

Figure 21. Power spectrum of static pressure near the suction surface, near leading edge (point A in figure 20).

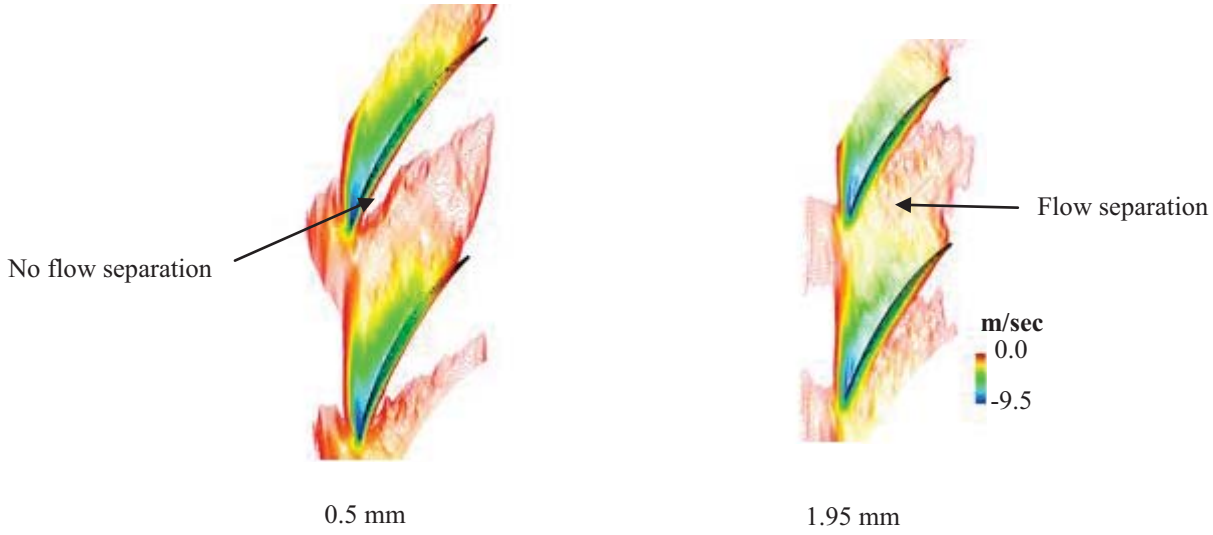

Figure 22: Comparison of time-averaged negative axial velocity contours, rotor tip, near stall.